ORIGINAL PAPER

Investigation and validation of solar photovoltaic-fed modular multilevel inverter for marine water-pumping applications

Dishore Shunmugham Vanaja[1] · Albert Alexander Stonier[2] · Geetha Mani[3] · Srinivasan Murugesan[2]

Abstract
This article discussed the development of a solar photovoltaic-fed modular multilevel inverter (MMI) with reduced switch count to operate an asynchronous motor drive for maritime applications. The proposed marine water-pumping system consist of a PV panel, an asynchronous motor drive, and modular inverter. The suggested topology can produce 11 levels of output using asymmetric DC sources. The proposed MMI consists of five DC sources, and they are powered by the PV panels. The primary advantage of the proposed topology is that it does not need any auxiliary circuit to produce the negative levels. Moreover, the active sources (PV panels) in the proposed system are reduced by implementing a modified single-input and multiple-output SEPIC converter. The power consumption by on-board pumping systems in maritime is estimated to be almost 50% of the total power. Taking this into account, this article investigates an adaptive fuzzy logic-based closed-loop control design for reducing the losses in the induction machine and thereby improving the efficiency of the system. Further, the performance of the proposed system is compared with the conventional PI controller, and from the results, it is proved that the proposed control system works effectively in reducing the losses as well as improving the efficiency of the system. The simulations are carried out in MATLAB/Simulink, and the experimental investigations are carried out in the laboratory. The obtained experimental results are similar to the simulation results.

Keywords Modular multilevel inverter · Asynchronous motor drive · Total harmonic distortion · Proportional/integral · Fuzzy controller

✉ Albert Alexander Stonier
ootyalex@gmail.com

Dishore Shunmugham Vanaja
dishore312@gmail.com

Geetha Mani
geetha.mani@vit.ac.in

Srinivasan Murugesan
srinieee@kongu.ac.in

1 Department of Electrical and Electronics Engineering, Rajadhani Institute of Engineering and Technology KTU University, Attingal 600115, India

2 Department of Electrical and Electronics Engineering, Kongu Engineering College, Perundurai 638060, India

3 School of Electrical Engineering, Vellore Institute of Technology, Vellore, India

1 Introduction

Globally, the naval and shipping industries have made significant initiatives to minimize airborne emissions and energy consumption. Certain rules governing the prevention of pollution and its effects in marine environment are strictly adhered by the International Convention for the Prevention of Pollution from Ships organization (MARPOL) [1, 2]. The use of diesel engines in ship can produce about 2.8% carbon dioxide (CO2), 15% of nitrogen oxides (NOX) and 13% of sulfur oxides (SOx), which are the primary pollutants and this leads to the emission of greenhouse gases and environmental issues [3]. The use of gasoline engines in ships leads to air pollution, and carbon dioxide emissions are gradually increasing, with the goal of reaching 8% by 2020 [4].

To fix the issues associated with atmospheric air pollution caused by the ship, a paradigm shift has continued to progress toward the installation of solar energy as a source of clean energy. Solar energy is currently the most popular alternative for the majority of marine applications because it
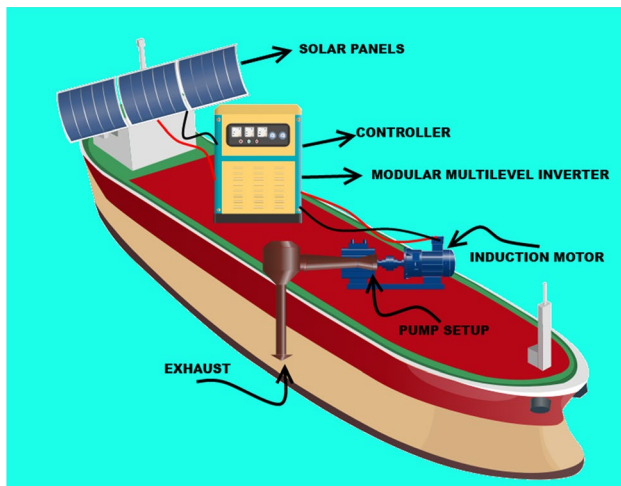
Fig. 1 Schematic diagram of the proposed system

Fig. 2 Proposed MMI

involves less maintenance, operates quietly owing to the unavailability of rotating components, and takes up less space on rooftops of ships. Energy produced from the sun energy is extracted using converters and inverters make the AC power to integrate with a wide variety of high-power loads [5].

In general, DC motors are often used in PV-based water-pumping systems. A common drawback in DC motor is that it requires regular maintenance of the commutators and brushes. Therefore, to compensate this drawback brushless DC motors are used in PV-based water-pumping systems. On the other hand, induction motor (IM) gives a better performance, maintenance free, and low cost when compared with other motors. Usually, the IM is controlled using the direct torque control (DTC) and the vector control or field-oriented control (FOC). The field-oriented control has a better and faster response, but the only drawback is that as there is variation in the torque and flux the control becomes complex. The use of hysteresis controller in the DTC method contributes to high ripples in torque and flux.

To reduce these ripples, multilevel inverters (MLIs) are used. The use of MLI decreases the efficiency of the system, since the MLI consist of more number of switches. To address this issue, the proposed system uses a MMI with reduced number of switches. In [6, 7], the authors proposed a modular multilevel inverter with reduce switch count. A cascaded control method is implemented for integrating the modular inverter to the grid. In [8], the authors presented a modular multilevel converter (MMC) for medium voltage DC systems in ship with combined storage system. The combined storage system consists of batteries and super capacitors for providing constant and uninterrupted power supply. The MMC uses decoupled control method for mitigation of voltage fluctuations and harmonics in the system.

In [9], the authors proposed a MMC for medium voltage DC systems in ship with nearest-level modulation (NLM) and hybrid NLM methods. From the results, it is concluded
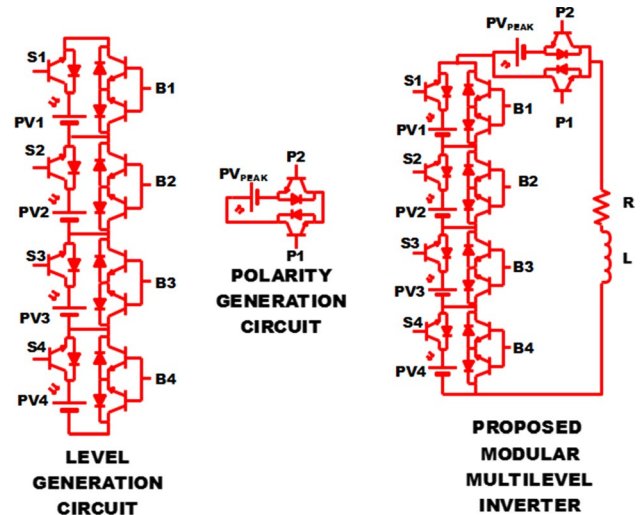
that the hybrid NLM method gives lesser THD than the conventional NLM method. A modular multilevel cascaded converter is developed in [10] for ship board power system. The MMCC has the capability to operate in buck and boost modes. Later as an application point of view, the MMCC is used in STATCOM for providing the reactive power.

In [11] a reduced switch 17-level MMI was proposed with NLM method. The suggested MMI is compared with the recent configurations. The proposed switching method provides a lesser THD when compared with SHE method. A symmetrical hybrid five-level topology is implemented in [12] to improve the power quality in ship power system. Fundamental frequency modulation is implemented for the proposed system to eliminate the harmonics and improve the power quality. In [13] the authors developed an advanced NPC converter using Si IGBT and SiC MOSFET for ship power system. Fundamental frequency modulation is implemented for the proposed system to eliminate the harmonics and improve the power quality.

The solar photovoltaic (PV)-fed asymmetric 11-level inverter illustrated in Fig. 1 employs intelligent control methods to achieve an excellent static and dynamic performance for maritime applications. The inverter supplies power to the electric motor that drives the ship's seawater cooling pump. With proportional/integral controllers and fuzzy controllers, the effectiveness of the MMI-fed IM drive is investigated. Due to improved peak overshoot as well as stability, the proportional/integral (PI) controller is frequently used in speed control applications.

The FLC is the easiest method of all intelligent controllers for controlling the speed of induction motors. Since the ship's water is normally pumped from dawn to dusk, the starting current and voltage of the IM must be maintained appropriately [14]. Instead of hysteresis controllers, a fuzzy

Table 1 Switching sequence of the proposed 11-level MMI

S1	S2	S3	S4	B1	B2	B3	B4	P1	P2	Output voltage (V_o)
✓	X	X	X	X	✓	✓	✓	✓	X	1 Vdc
✓	✓	X	X	X	X	✓	✓	✓	X	2Vdc
✓	✓	✓	X	X	X	X	✓	✓	X	3 Vdc
✓	✓	X	✓	X	X	✓	X	✓	X	4 Vdc
✓	✓	✓	✓	X	X	X	X	✓	X	5 Vdc
X	X	X	X	✓	✓	✓	✓	✓	X	0 Vdc
X	✓	✓	✓	✓	X	X	X	X	✓	−1 Vdc
X	X	✓	✓	✓	✓	X	X	X	✓	−2Vdc
X	X	X	✓	✓	✓	✓	X	X	✓	−3 Vdc
✓	X	X	X	X	✓	✓	✓	X	✓	−4 Vdc
X	X	X	X	✓	✓	✓	✓	X	✓	−5 Vdc

Table 2 Parameters of the proposed 11-level MMI

Parameters	Based on number of levels	Based on number of modules
Number of levels	N_L	$11n$
Number of switches	$(N_L + 3)$	$11n + 3$
Number of diodes	$(N_L + 3)$	$11n + 3$
Number of drive circuit	$(N_L - 1)$	$10n$
Number of DC sources	$(N_L - 6)$	$5n$
Total standing voltage (TSV)	$(N_L + 3)$	$14n$

logic block is used, along with a switching selection table, to reduce flux and torque ripples. Fuzzy control is robust, well-suited for nonlinear control strategies and does not require knowledge of the precise model.

The objectives of the proposed work are:

- Design a modular multilevel inverter with reduced switches
- Design a modular converter for effective utilization of the DC sources
- Design a fuzzy logic-based DTC control method to enhance the power quality in the marine power system
- Real-time execution of the proposed inverter-fed IM drive using FPGA controller (SPARTAN3E500)

This article is mostly concerned with the functioning of MMI fed with IM for maritime applications. This article is organized as follows: Section 2 covers the design of MMI, modes of operation, and the parameters of MMI. Section 3 focuses on the design of SIMO (single-input and multiple-output) SEPIC converter, design of IM and the design of water pump. Section 4 presents the control strategy for the proposed system. Section 5 presents the simulation results and Section 6 presents the experimental results.

2 Proposed system design

Modular multilevel inverter (MMI) is an important achievement to the development of MLI configurations. For medium- or high-power implementations, it has become an attractive topology. Even though many structures have so far been developed based on the reduced number of components, some structures are still in progress.

The implementation of MMI is much essential to maintain a good quality of power in the power system. Due to the nonlinear characteristics of the traditional inverters, the output power cannot meet the IEEE grid code specifications. Therefore, LC filters are applied on the output side of the traditional inverters to remove harmonics and progress the power quality. While stress on the switches is typically not minimized, the system's reliability and performance are decreased [15]. The issues of the traditional inverters can be solved by using multilevel inverters. However, when the output tends to increase, the switching elements also increase in a conventional MLI.

As the amount of switching components increases, the associated gate drivers also increase. Accordingly, switching the components become difficult and affect the efficiency of the inverter. Moreover, the losses of the inverter also increase. The construction of reduced device count MLIs is additionally a practice aimed at reducing both production costs and energy costs indirectly due to on–off losses and related heat sinks. When assessed with the conventional MLIs, the reduced part count configurations greatly decrease the switch count because of implementing the switches in different patterns.
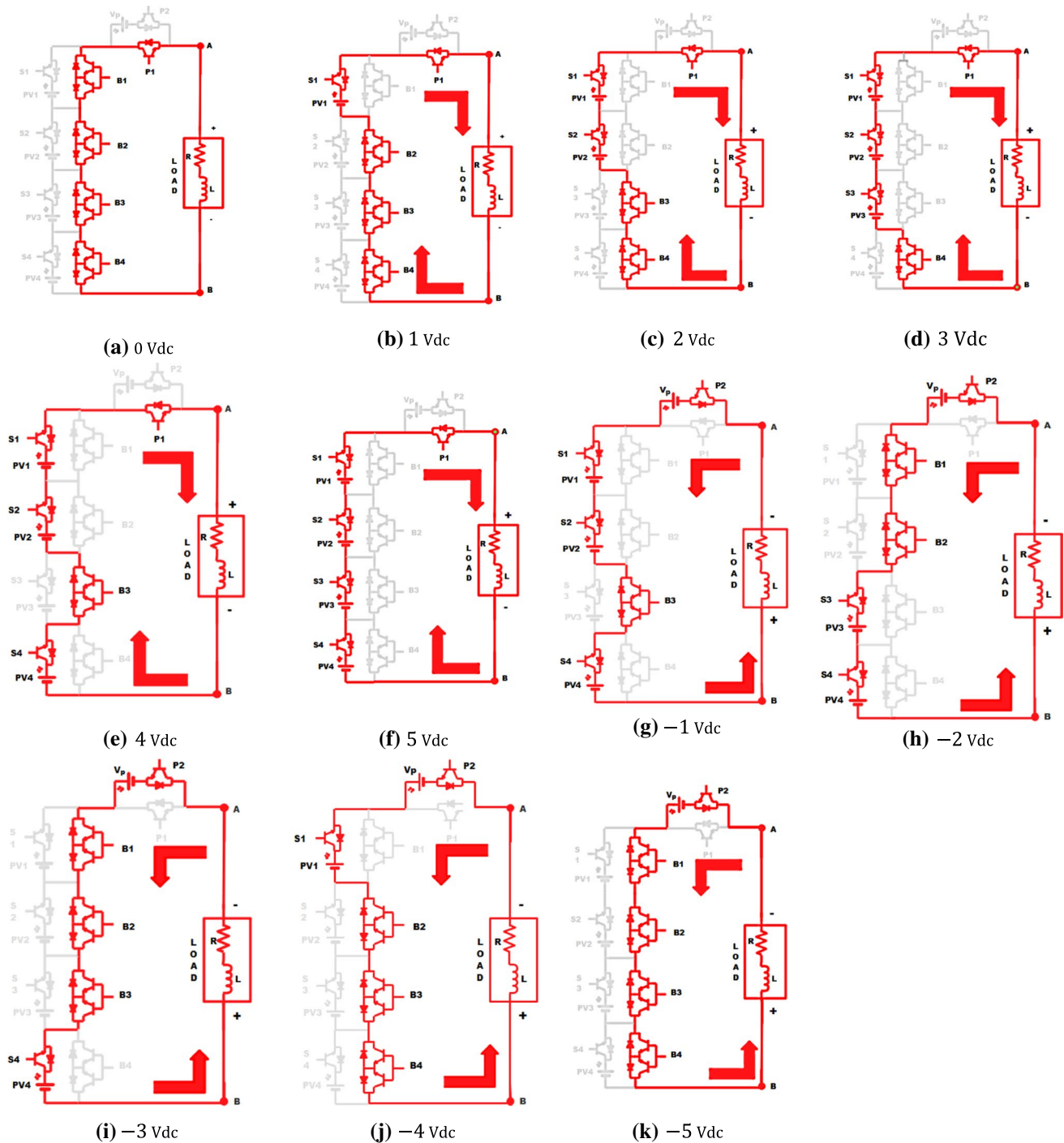
(a) 0 Vdc   **(b)** 1 Vdc   **(c)** 2 Vdc   **(d)** 3 Vdc

(e) 4 Vdc   **(f)** 5 Vdc   **(g)** −1 Vdc   **(h)** −2 Vdc

(i) −3 Vdc   **(j)** −4 Vdc   **(k)** −5 Vdc

Fig. 3 Modes of operation

The MLI-HDBK-2017F [16] standard cites that increased device count affects the reliability of the inverter. In any power electronic system, the system efficiency is inversely correlated with the device part count. Reducing the devices increases the stability and also boost system performance.

Therefore, power electronic systems with reduced component count improve the durability and effectiveness of the system.

Figure 2 shows the structure of the proposed MMI. A 11-level asymmetric modular multilevel inverter (AMMI)
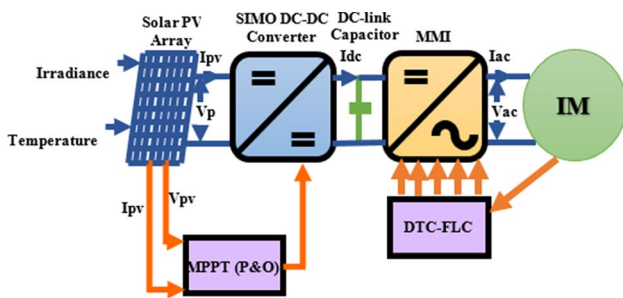
Fig. 4 Block diagram of the proposed system
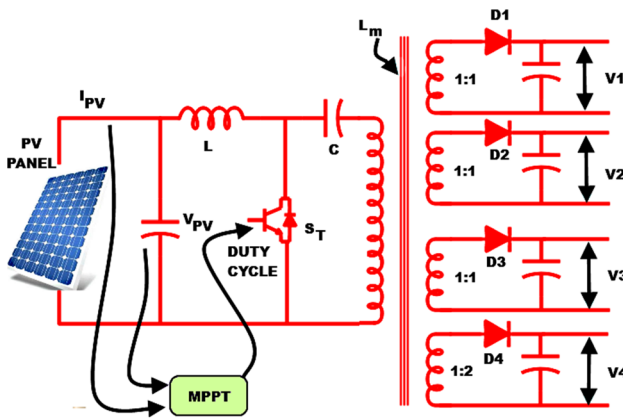
Fig. 5 Simo SEPIC converter

is produced in the same symmetric structure when the input DC power supply is $1:1:1:2:V_p$. There are 14 switches in the suggested structure of which 6 are unilateral switches and 4 are bilateral switches. The suggested structure contains five input DC sources. The fifth-input DC source (V_p) is responsible for producing the negative levels in the suggested structure.

Therefore, V_p value is selected as the total magnitude of all the four independent DC inputs. In the suggested 11-level inverter the V_p is $5V$ by considering $(1V + 1V + 1V + 2V = 5V)$. Table 1 indicates the triggering method for the 11-level AMMI. The power switches are intelligently designed to get the possible voltage levels. Five positive, five negative, and zero level combine to form a 11-level. The positive five level is generated by triggering the switches S1 to S4, B1 to B4 randomly along with switch P1. To generate the negative five level in the suggested configuration, the switches S1 to S4, B1 to B4 are randomly switched along with switch P2. By switching all the bidirectional switches along with switch P1, the zeroth level is produced. Table 2 presents the parameters of the suggested

Table 3 Parameters of the SIMO boost converter

Parameters	Value
Input PV voltage	35 V
Inductance	6.4 mH
Capacitance	47μF
Duty cycle	0.735
Switching frequency	50 kHz
Output voltage	336 V

Table 4 Specifications of the IM

Parameters	Specifications
Nominal power	3.5 kw
Nominal speed (ωr)	1500 rpm
Number of poles (P)	4
Phase voltage of stator (V)	230
Per phase rotor resistance (Rr)	0.69 Ω
Per phase stator resistance (Rs)	0.595 Ω
Leakage inductance of rotor per phase (Llr)	0.00301 H
Leakage inductance of stator per phase (Lls)	0.00301 H
Per phase magnetizing inductance (Lm)	0.08512 H
Inertia of rotor (J)	0.011 kgm^2
Frequency (f)	50 Hz

topology. The parameters presented in Table 2 is designed by considering the number of levels (N_L) and sectional units or modules (n). Higher voltage levels can be generated by the suggested configuration when connected in cascaded form. When two 11-level AMMI structures are connected in the cascaded manner, a 21-level (10 positive level, 10 negative level, and zero level) is generated at the output. The modes of operation of the suggested 11-level AMMI are displayed in Fig. 3.

3 Design of the proposed system

The proposed system consists of solar PV panels, SIMO DC–DC converter, MMI, IM, and centrifugal pump. Figure 4 presents the block diagram of the proposed system.

3.1 Design of PV system

The solar PV system with a peak power rating of 150 W at STC (1000 W/m^2, 25 °C) is sufficient to drive the IM which is coupled with the centrifugal pump [17]. A 10-W solar photovoltaic specification defines 36 cells wired in series, each with a voltage of 0.588 V. The ratings of the photovoltaic panel are

maximum power ($P_{max} = 10 W_p$), panels open-circuit voltage ($V_{oc} = 21.6$ V), and panels short-circuit current ($I_{sc} = 0.659$ A). To gain the optimum power capacity of 150 W, five 10 W panel and five 20 W panel are connected in series and parallel configuration. Equation (1) presents the current passing through the solar cells and it has four unknown parameters (I_L, I_0, R_s, and α) which have to be found before achieving the *V–I* characteristics of the solar photovoltaic cell [18, 19].

$$I = I_L - I_D = I_L - I_0 e^{\left(\frac{V + iRs}{\alpha}\right)} - 1 \tag{1}$$

A. Assessment of light current (I_L)

Equation (2) presents the light current I_L of the PV panel.

$$I_L = \frac{\phi}{\phi_{ref}}\left[I_{L,ref} + \mu_{I,SC}(T_C - T_{C,ref})\right] \tag{2}$$

B. Assessment of saturation current (I_0)

Equation (3) presents the saturation current of the PV panel

$$I_0 = I_{0,ref}\left(\frac{T_{C,ref} + 273}{T_C + 273}\right)^3 \exp\left[\frac{e_{gap}N_s}{q\alpha_{ref}}\left(1 - \frac{T_{C,ref} + 273}{T_C + 273}\right)\right] \tag{3}$$

Throughout the reference situation, the saturation current can be estimated as,

$$I_{0,ref} = I_{L,ref} \exp\left(-\frac{V_{oc,ref}}{\alpha_{ref}}\right) \tag{4}$$

C. Estimation of TVTC factor

Temperature is the focus of the thermal voltage timing completion factor (α), which is obtained as:

$$\alpha_{ref} = \frac{2V_{mp,ref} - V_{oc,ref}}{\frac{I_{sc,ref}}{I_{SC,ref} - I_{mp,ref}} + \ln\left(1 - \frac{I_{mp,ref}}{I_{SC,ref}}\right)} \tag{5}$$

$$\alpha = \frac{T_C + 273}{T_{C,ref} + 273}\alpha_{ref} \tag{6}$$

D. Estimation of series resistance (RR_s)

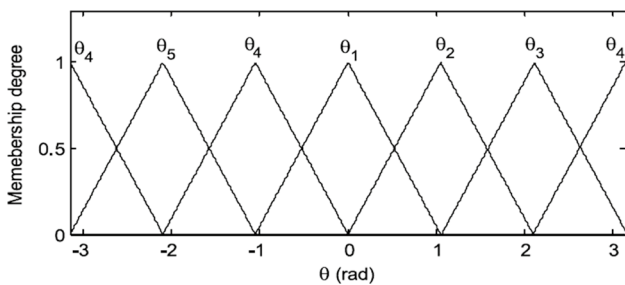**Fig. 6** Membership function of flux position

The series resistance is obtained by Eq. (7).

$$R_s = \frac{\alpha_{ref} \ln\left(1 - \frac{I_{mp,ref}}{I_{SC,ref}}\right) + V_{OC,ref} - V_{mp,ref}}{I_{mp,ref}} \tag{7}$$

3.2 Design of Simo boost converter

Figure 5 illustrates a single-input and multiple-output dc–dc boost converter sandwiched between the photovoltaic arrays and the suggested inverter. This converter generates four isolated direct current sources in the proportion 1:1:1:2. This converter is powered by a single solar photovoltaic panel, which eliminates unbalanced voltages and step size variations caused by a variety of environmental conditions.

The inductance's magnitude can be determined using the relationship:

$$L = \left(\frac{m_i V_{Pv}}{4af_s I_r}\right) \tag{8}$$

where V_{Pv} is the input PV voltage, m_i is the modulation index, f_s is the switching frequency, I_r is the ripple current, and *a* is the overloading factor, normally considered as 1.25.

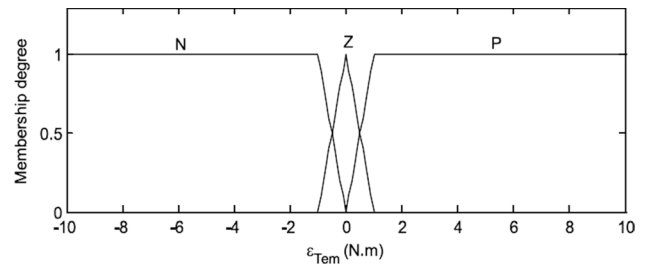The capacitance value can be determined by using the following relationship:

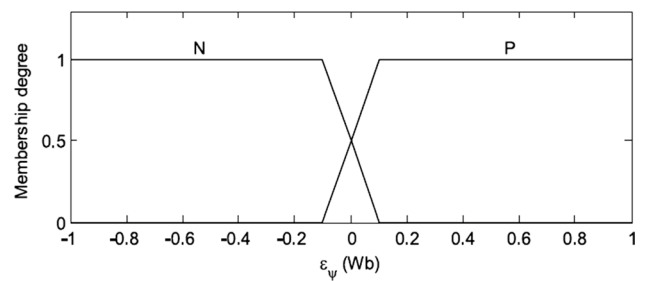**Fig. 7** Membership function for electromagnetic torque error
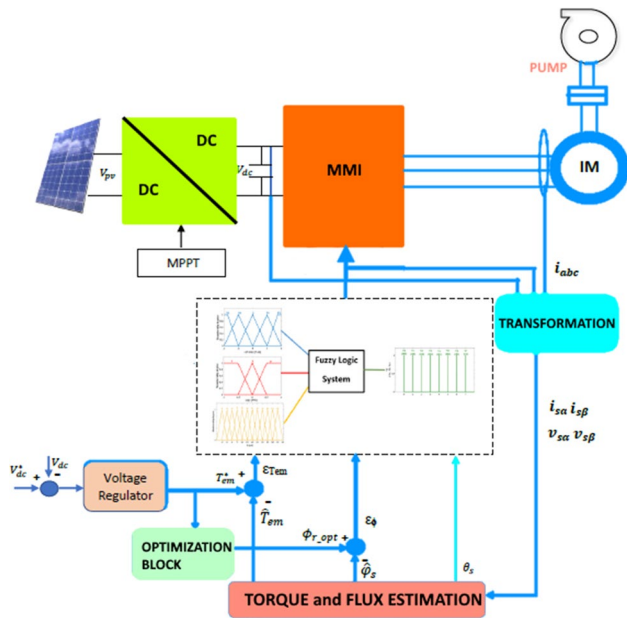

Fig. 8 Membership function for flux linkage error

Fig. 9 FLC-based DTC Control of IM

Table 5 Fuzzy rules

e/ce	NB	NS	ZE	PS	PB
NB	ZE	NS	NB	NB	NB
NS	ZE	NS	NB	NS	NB
ZE	PB	PS	ZE	NS	NB
PS	PB	PS	PS	ZE	NS
PB	PB	PB	PB	PS	ZE

$$C = \left(\frac{DI_{pv}}{V_{pv} r f_s \times 0.5} \right) \tag{9}$$

where I_{pv} is the PV current, r is the ripple voltage, D is the duty cycle.

The duty cycle value can be determined by using the following relationship:

$$D = \frac{V_{out}}{V_{out} + V_{PV}} \tag{10}$$

The speciation's of the boost converter are represented in Table 3.

3.3 Design of induction motor

The IM dynamic equations in the reference α–β can be reported as follows:

The stator equations in α–β coordinate system:

Stator voltages
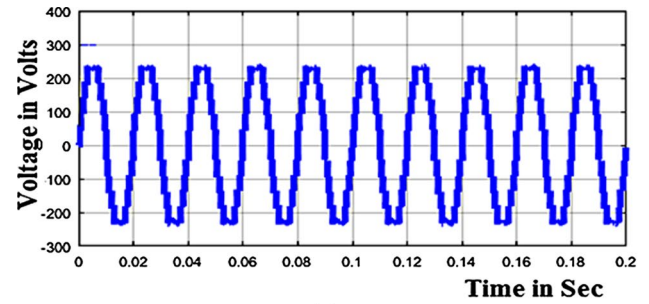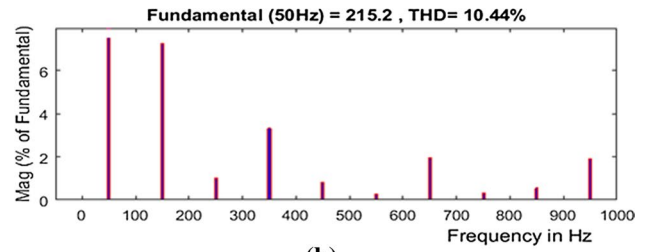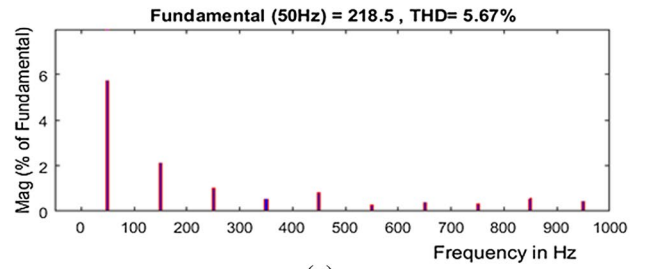
Fig. 10 **a** Output voltage waveform **b** THD obtained using PI controller **c** THD obtained using FLC-DTC controller of an 11-level inverter
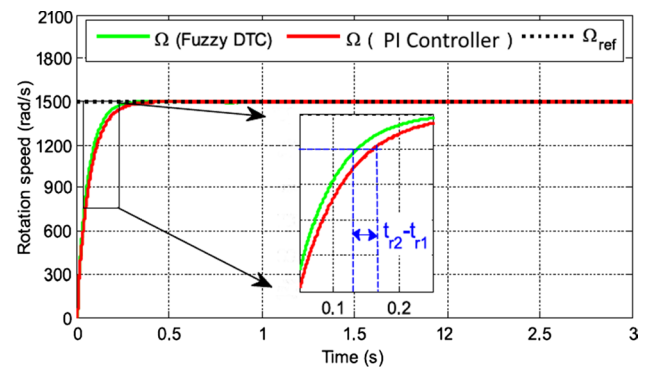

Fig. 11 Speed of the IM

$$\begin{aligned} V_{\alpha s} &= R_s I_{\alpha s} + \frac{d}{dt} \phi_{\alpha s} \\ V_{\beta s} &= R_s I_{\beta s} + \frac{d}{dt} \phi_{\beta s} \end{aligned} \tag{11}$$
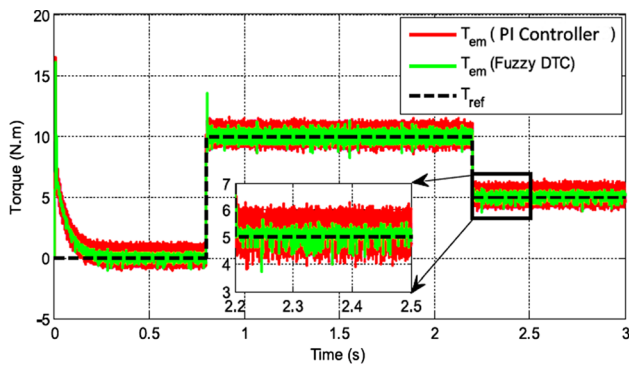
Stator flux

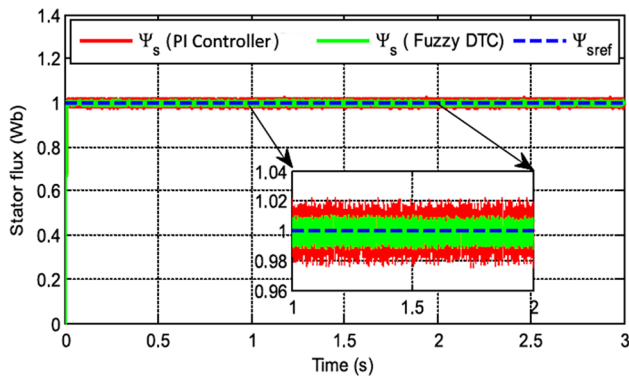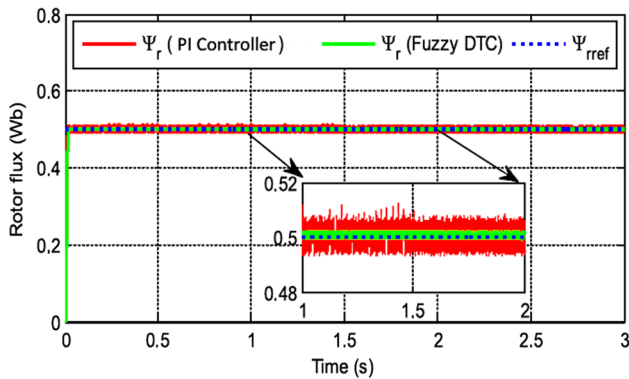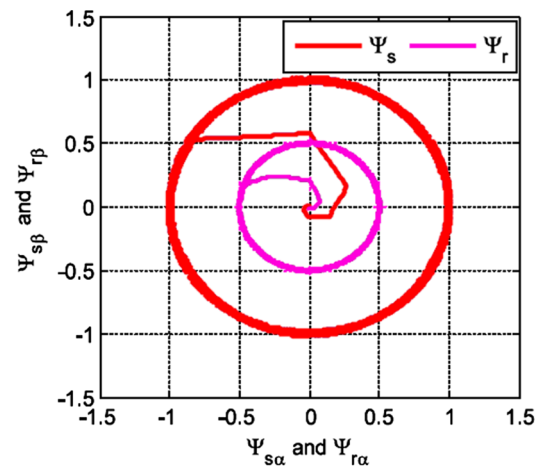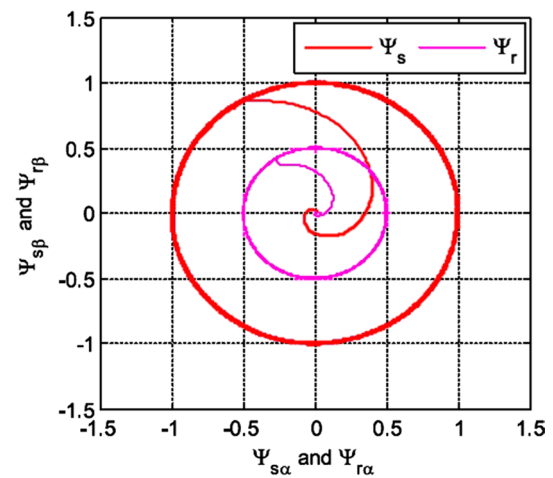**Fig. 12** Electromagnetic torque of the IM

Fig. 13 Stator flux

Fig. 14 Rotor flux

$$\phi_{\alpha s} = l_s I_{\alpha s} + M I_{\alpha s}$$
$$\phi_{\beta s} = l_s I_{\beta s} + M I_{\beta s} \tag{12}$$

The rotor equations α–β coordinate system:
Rotor voltages

(a)

(b)

Fig. 15 Progression of stator and rotor flux using; **a** PI control; **b** fuzzy control

$$0 = R_r I_{\alpha r} + \frac{\mathrm{d}}{\mathrm{d}t}\phi_{\alpha r} + w_m \phi_{\beta r}$$
$$0 = R_r I_{\beta r} + \frac{\mathrm{d}}{\mathrm{d}t}\phi_{\beta r} + w_m \phi_{\alpha r} \tag{13}$$

Rotor flux

$$\phi_{\alpha r} = l_r I_{\alpha r} + M I_{\alpha r}$$
$$\phi_{\beta r} = l_r I_{\beta r} + M I_{\beta r} \tag{14}$$

and the electromagnetic torque developed:

$$T_{em} = \frac{3}{2}P\big(\phi_{\alpha s}I_{\beta s} - \phi_{\beta s}I_{\alpha s}\big) \tag{15}$$

where l_r stator and rotor inductances, M: mutual inductance, stator and rotor currents, Rr: Stator and Rotor resistances.

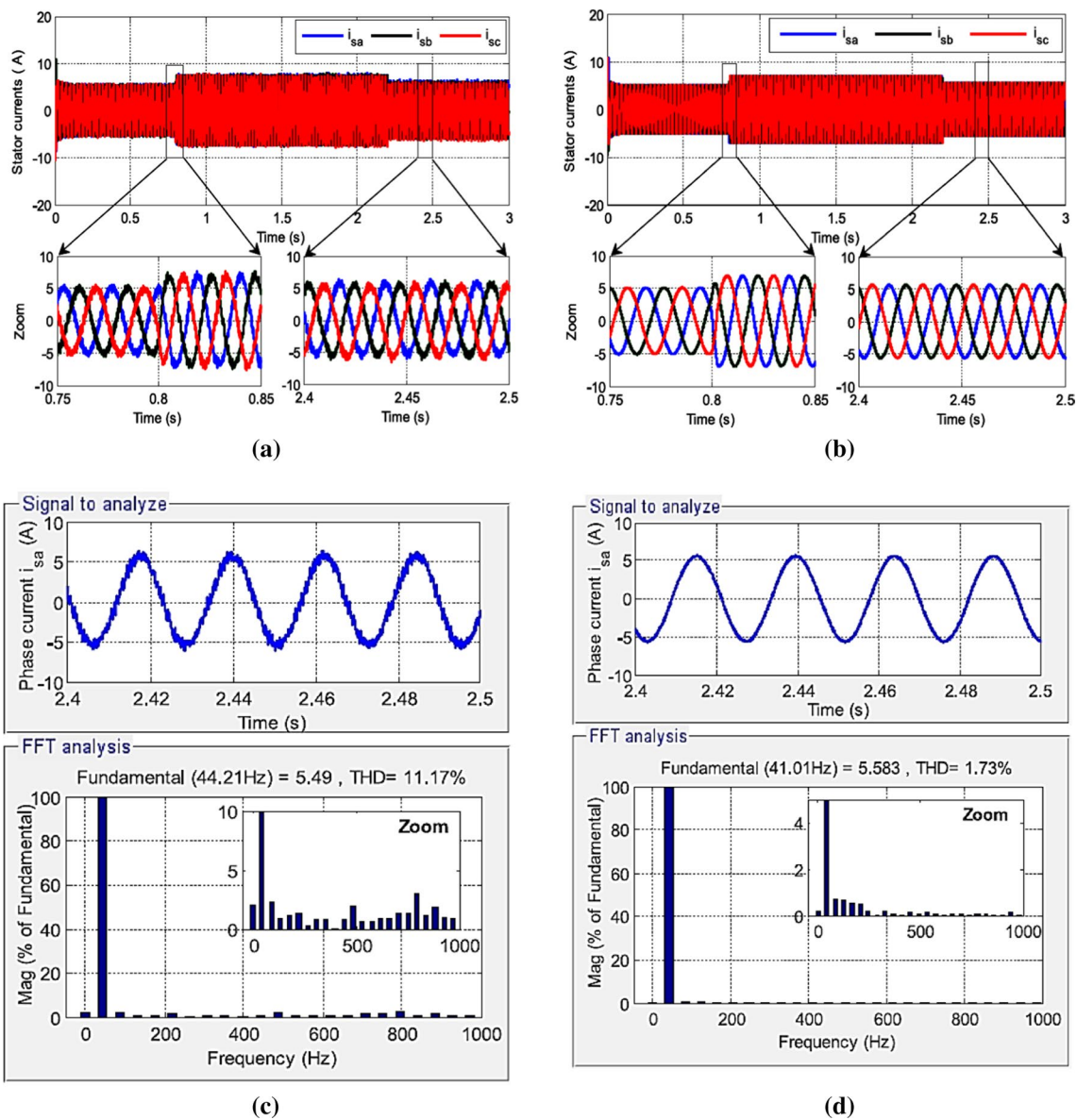Table 4 presents the specifications of the IM.

Fig. 16 Progression of stator current using; **a** PI control; **b** fuzzy control; **c** THD of stator current with PI control; **d** THD of stator current with fuzzy control

3.4 Design of water pump

IM drive and centrifugal pump are combinedly used in the water pumping system. Pump affinity law is suggested as a standard by which centrifugal pumps are designed. The load torque is proportional to the square of the speed according to the equation, as stated in (16).

$$T_L = K_p \times \omega_r^2 \tag{16}$$

$$K_p = \frac{9.94}{(2 \times \pi \times 24)^2} = 0.00043712 \text{ Nm/(rad/sec)}^2.$$

4 Control strategy of the proposed system

To enhance the system's performance and minimize electromagnetic torque and flux ripples, a fuzzy logic controller (FLC) is implemented in place of the hysteresis controller and conventional switching tables. The flux error, torque error, and flux angle are assumed as inputs to the FLC in the proposed system. The FLC is able to determine the required inverter vector state. The expression of the stator flux components can be written as:
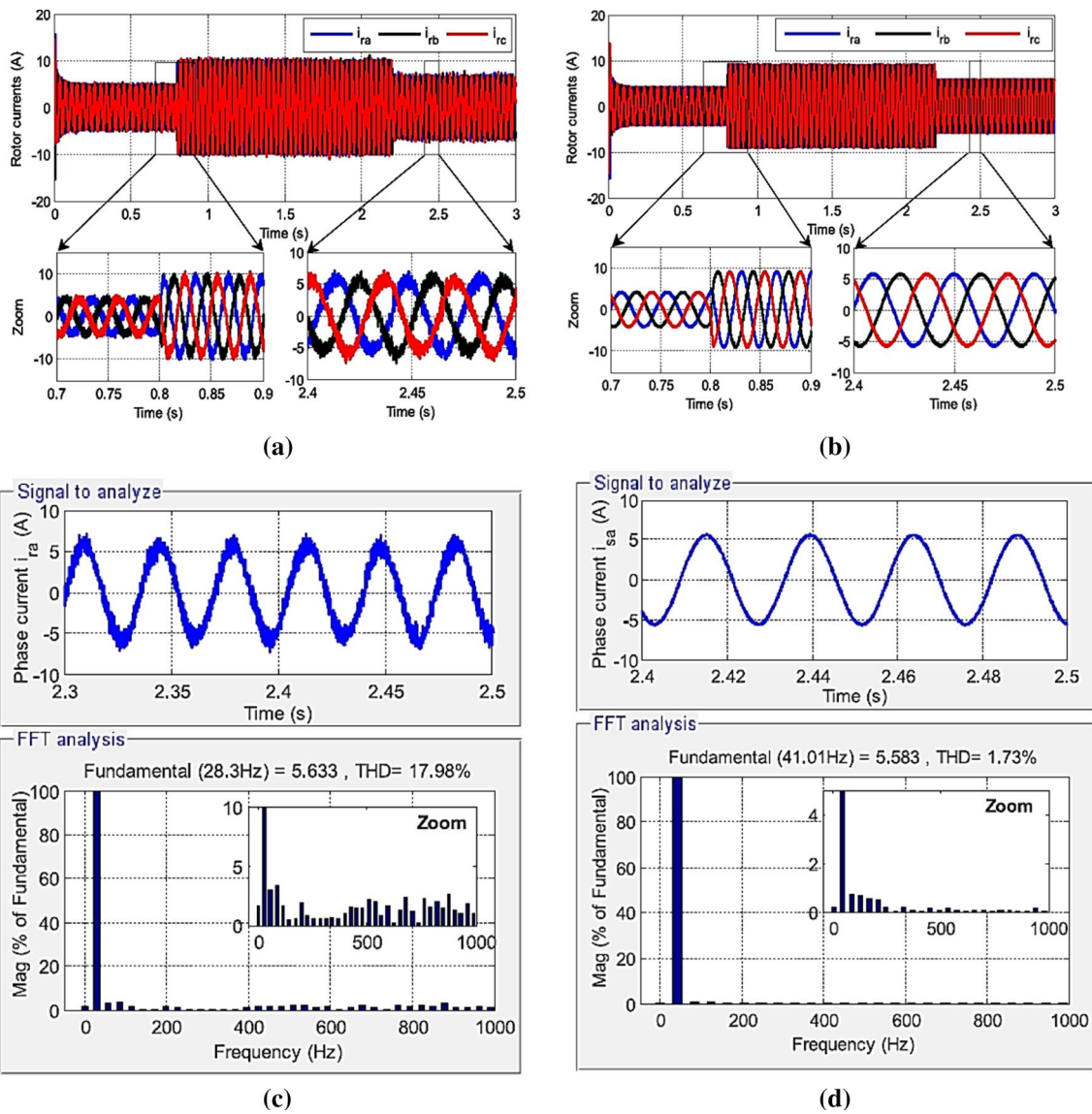
Fig. 17 Progression of rotor current using **a** PI control; **b** fuzzy control; **c** THD of rotor current with PI control; **d** THD of rotor current with fuzzy control

Table 6 Comparison of PI and fuzzy control

Parameters	PI	Fuzzy	%↑
Rise time of the speed (s)	0.159	0.130	18.23
Torque distortions (N m)	2.03	1.01	50.24
Flux distortions in stator (Wb)	0.05	0.03	40
Flux distortions in rotor (Wb)	0.012	0.003	75
THD of the stator current (%)	11.17	1.73	85
THD of the rotor current (%)	17.98	2.81	84

↑ −improvement

$$\begin{cases} \hat{\varphi}_{s\alpha} = \int_0^t \left(v_{sa} - R_s \cdot i_{sa} \right) \cdot \mathrm{d}t \\ \hat{\varphi}_{s\beta} = \int_0^t \left(v_{s\beta} - R_s \cdot i_{s\beta} \right) \cdot \mathrm{d}t \end{cases} \quad (17)$$

The estimated electromagnetic torque can be expressed by:

$$\hat{T}_{em} = p \cdot \left(\hat{\varphi}_{s\alpha} \cdot i_{s\beta} - \hat{\varphi}_{s\beta} \cdot i_{s\alpha} \right) \quad (18)$$

Moreover, the amplitude and the stator flux angle are determined by:

Fig. 18 Experimental setup of PV panels with MMI

$$\hat{\varphi}_s = \sqrt{\hat{\varphi}_{s\alpha}^2 + \hat{\varphi}_{s\beta}^2}$$
$$\theta_s = \mathrm{arctg}\left(\frac{\hat{\varphi}_{s\beta}}{\hat{\varphi}_{s\alpha}}\right) \tag{19}$$

In general, FLC consists of three stages: fuzzification, the use of guidelines to evaluate the outcome depending on the input data, and defuzzification. By characterizing the membership functions for every input parameter, the fuzzification process converts predetermined input parameters to linguistic parameters. The positioning of flux is the first input parameter. This input parameters discourse universe is comprised of five fuzzy sets ($\theta 1$–$\theta 5$), the membership functions of which are represented in Fig. 6.

The second input is an electromagnetic torque error, and its discourse universe is grouped into three fuzzy sets: positive torque error (P); zero torque error (Z); negative torque error (N). The trapezoid membership functions for the fuzzy sets (P) and (N) are illustrated in Fig. 7. The third input parameter as presented in Fig. 8 is the flux error; its discourse universe is split into 2 fuzzy sets: positive flux error (P) and negative flux error (N). Figure 9 presents the FLC control of IM. Table 5 presents the fuzzy rules of the fuzzy controller.
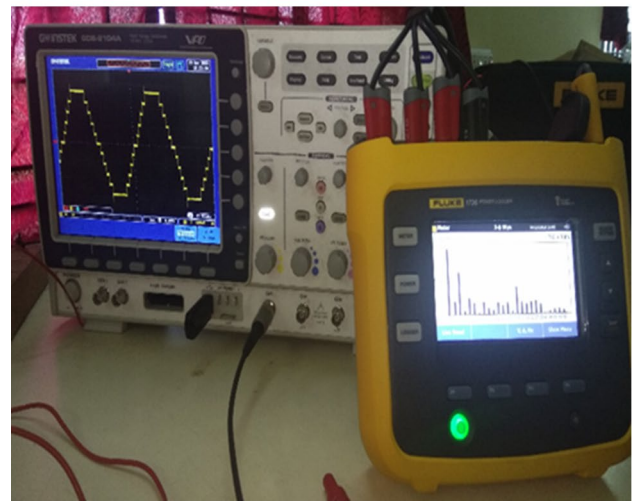
A. Interference

The inference method is conducted using Mamdani's method. The factor of weighting for ith rule (αI) is expressed by:

$$\alpha i = \min\left(\mu Ai(e\varphi), \mu Bi(eT), \mu Ci(\theta)\right) \tag{20}$$

$$\mu\prime V(V) = \max\left(\alpha i, \mu Vi(V)\right) \tag{21}$$

(a)

(b)

Fig. 19 Prototype of **a** MMI; **b** DSO and Fluke power analyzer
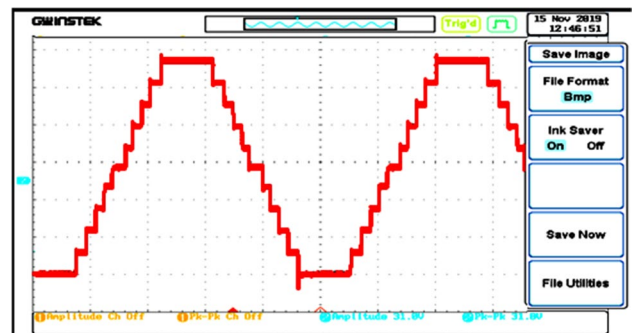
Fig. 20 Experimental output of 11-level MMI
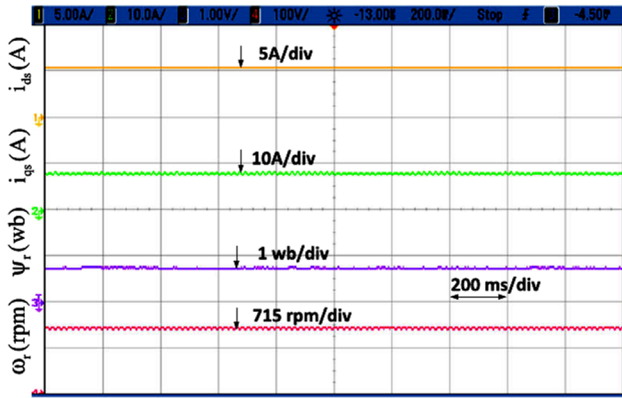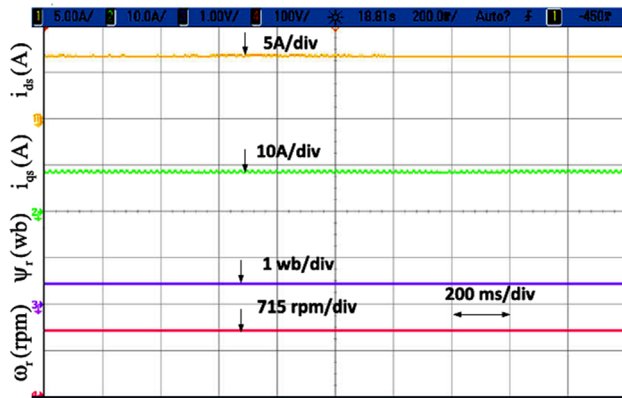
Fig. 21 Steady-state performance using; **a** PI controller; **b** fuzzy controller

Fig. 22 Transient state performance for case 1 using; **a** PI controller; **b** fuzzy controller

where $\mu Ai\ (e\varphi)$ the membership value of flux error, $\mu\ (eT)$ the membership value of torque error, $\mu\ (\theta)$ the membership value of stator flux angle.
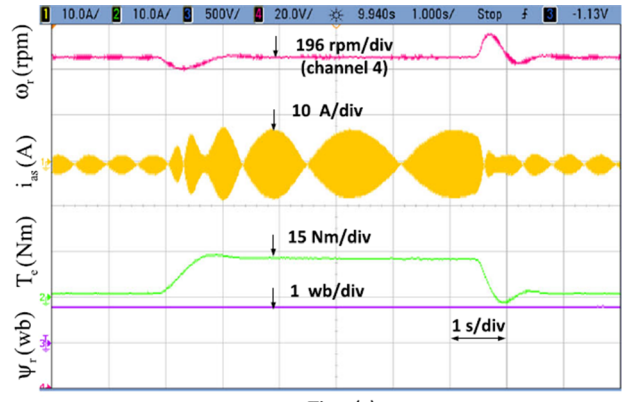
B. Defuzzification

The max method expressed by Eq. (21) has been used to converter the fuzzy values into crisp values.
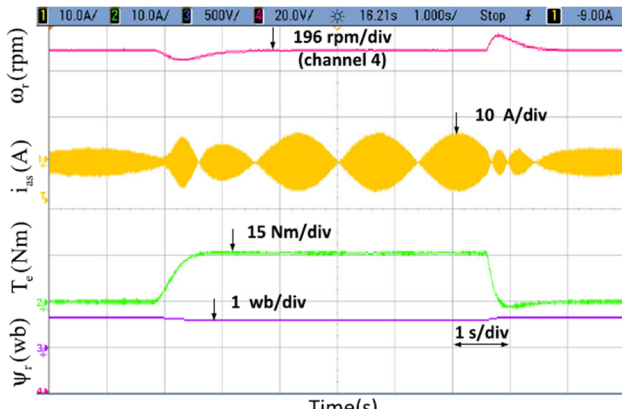
$$\mu'Vou(V) = \max\ i = 1$$

$$180\ \max\ \left(\mu'Vi(V)\right)$$

5 Simulation results

The proposed system is simulated using MATLAB/ Simulink 2021a. The proposed system is tested using the FLC and PI controller. Figure 10 presents the output of the

proposed 11-level MMI with its THD using both PI and FLC controller. Figures 11 and 12 present the speed and torque of the proposed system using PI and FLC controller. As indicated in Figs. 10 and 11, the system's rotating speed and the electromagnetic torque incorporate their references, with the FLC control having an ultra-fast processing time of almost 0.25 s and a lower rise time than the conventional PI control. Additionally, both control systems demonstrates that the load torque has no influence on the reactivity of the system's speed.

Figures 13 and 14 present the flux vectors of stator and rotor. From Fig. 13, it is observed that the stator flux guides the reference flux at 1Wb. From Fig. 14, it is observed that the rotor flux guides the reference flux at 0.5Wb. In the case of fuzzy DTC control, the machine's electromagnetic torque and flux exhibit low fluctuations in comparison with PI control. Similarly, the stator and rotor flux paths presented in Fig. 15 are more concentric than those acquired using the PI controller. Additionally, it is noted that fluctuation in the
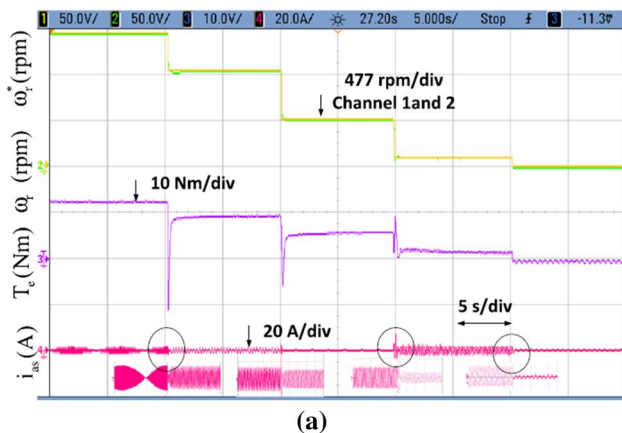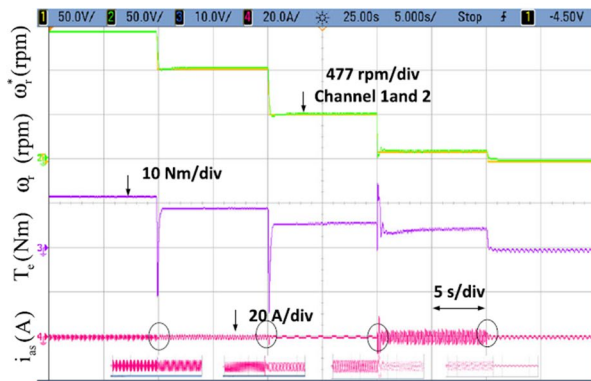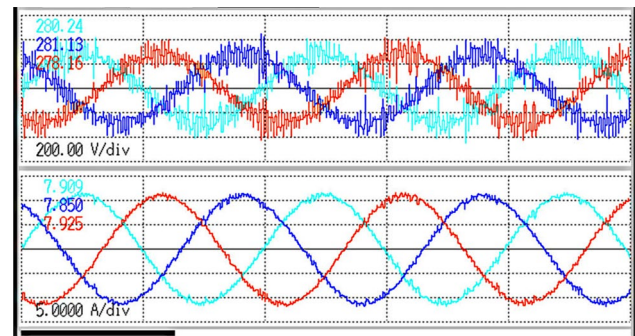
Fig. 23 Transient state performance for case 2 using; **a** PI controller; **b** fuzzy controller

Fig. 24 Experimental output of **a** stator voltage and stator current; **b** THD of stator voltage and stator current using PI controller
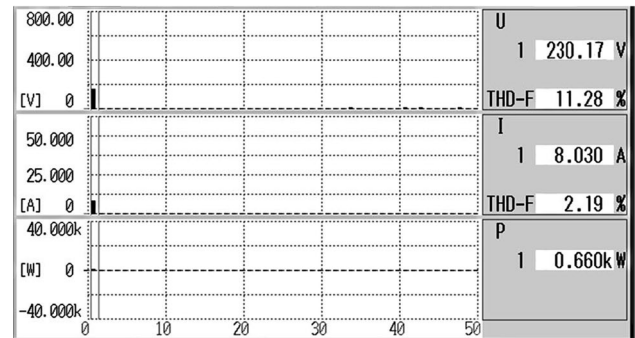
torque has no effect on the flux, indicating that the torque and the flux are decoupled.

Figure 16 presents the waveforms of stator currents and their respective THDs using PI and fuzzy control. From Fig. 16a and b, it is observed that the three-phase stator current waveform obtained using the PI control appears to be non-sinusoidal and produces a THD of 11.17%, whereas the waveform obtained using the fuzzy control appears to be sinusoidal and produces a THD of 1.73%. Figure 17 presents the waveforms of rotor currents and their respective THDs using PI and fuzzy control.

From Fig. 17a and b, it is observed that the three-phase rotor current waveform obtained using the PI control appears to be non-sinusoidal and produces a THD of 17.98%, whereas the waveform obtained using the fuzzy control appears to be sinusoidal and produces a THD of 2.81%. The variation in load torque causes changes in the flux which introduces harmonics in the system. Since the frequency of stator and rotor currents are proportional to the reference speeds, the fuzzy controller responds fast for these fluctuations and lowers the harmonics or torque

ripples. Therefore, the fuzzy controller works superior than the PI controller and improves the power quality of the system. Table 6 presents the comparative analysis of the proposed system using PI and fuzzy control.

6 Experimental results

In the experimental procedure, a modular multilevel inverter and an induction motor drive is linked to a solar PV array. Figure 18 presents the experimental setup of the PV panels with the MMI. Figure 19 presents the prototype of the MMI with DSO and fluke power quality analyzer. The pulses to the proposed inverter are fed using FPGA Spartan-6 controller. The IM is fed by MMI using 14 IGBTs and 10 gate drivers. The proposed MMI uses common emitter configuration of bidirectional switches which need only one driver circuit for its operation.

Therefore, the cost of the MMI is reduced. Moreover, the IGBT modules are compact in nature so the overall size of the MMI is reduced. Due to their compact feature, MMIs can be fitted at the back of the PV panel. Therefore, the MMI does not cover any additional space for its implementation. The motor currents are measured and the error
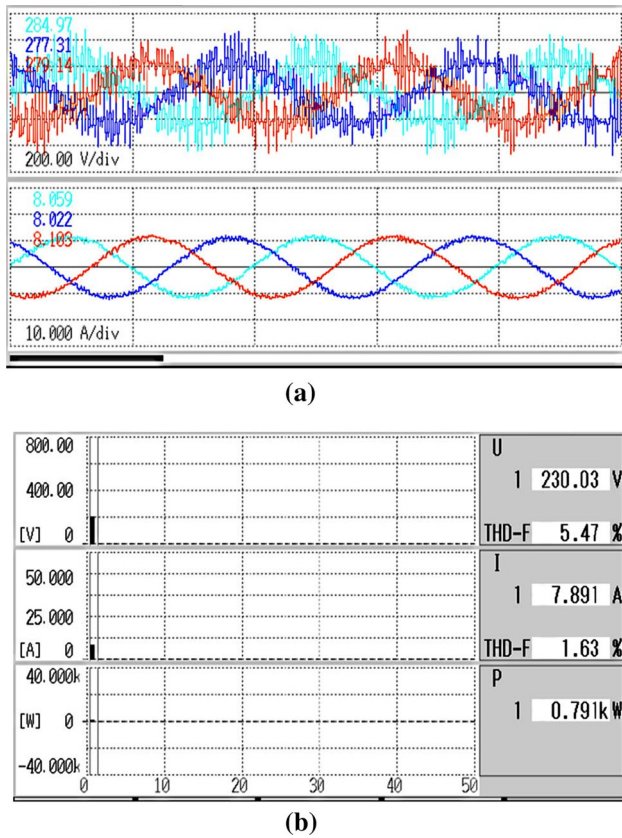
(a)

(b)

Fig. 25 Experimental output of **a** stator voltage and stator current; **b** THD of stator voltage and stator current using fuzzy controller

is sent as feedback to the controller to produce the PWM pulse to the MMI.

Figure 20 presents the experimental output of the 11-level MMI. The proposed work is examined experimentally and the results are compared with other related works. During the steady-state condition, the motor is operated at its rated speed with 85% of load.

Figure 21a and b presents the steady-state behavior of the system using PI and fuzzy controllers. From the waveforms in its observed that the ripple content present in the waveforms (flux, rotor speed, and the quadrature axis current)

obtained using the fuzzy controller are very less when compared with the waveforms obtained using the PI controller. Two cases are considered when the system is operating in the transient state condition. The first case is when there is a sudden change in load and the second case is when there is sudden change in the reference speed. When the motor runs at a rated speed of 1500 rpm and with 85% of load a sudden disturbance is introduced and its performance is observed using PI and fuzzy controller. Figure 22a and b presents the transient state behavior of the system using PI and fuzzy controllers. From the figures, it is observed that due to change in load (no load to full load) there exists a drop in speed of 92 rpm, and it recovers in 1.2 s using a PI controller, whereas the drop in speed is 70 rpm, and it recovers in 0.52 s using fuzzy controller. Due to sudden removal of load, overshoot occurs in the system and time taken by the PI controller to recover from overshoot is 1 s, whereas the time taken for the fuzzy controller is 0. 8 s. Figure 23a and b presents the transient behavior of the system regarding change in reference speed. The reference speed is varied step by step from 1500 rpm to 0. From the figures, it is observed that the fuzzy control acts fast and accurate than the PI controller. Figure 24 presents the experimental output of the stator voltage and current with its THD using PI controller, and Fig. 25 presents the experimental output of the stator voltage and current with its THD using fuzzy controller.

From Figs. 24 and 25, it is observed that the PI controller produces a voltage and current THD of 11.28% and 2.19%, whereas the fuzzy controller produces a voltage and current THD of 5.47% and 1.63%. Table 7 presents the comparison of the proposed system with other related works. Therefore, the fuzzy controller mitigates the harmonics and improves the power quality at the output of MMI.

7 Conclusion

This paper presents an investigation on a solar PV-fed MMI for the speed control of induction motor drive to evaluate the applicability of the system for water pumping applications in the marine sector. The suggested MMI uses common emitter

Table 7 Comparison of the proposed control system with other related works

Reference	[20]	[21]	[22]	Proposed
Method	Field-oriented control (FOC)	Sliding mode control (SMC)	Conventional direct torque control (DTC)	Fuzzy direct torque control (FDTC)
Response time (s)	0.492	0.2	0.35	0.163
Rise time (s)	0.175	0.101	0.175	0.1
Torque ripple (N.m)	2.49	2.32	2.20	1.11
Controllable Parameter	Current	Current	Ψ and T_{em}	Ψ and T_{em}
Durability	Non-durable	Non-durable	Durable	Durable

design of bidirectional switches that will need a single driver circuit for its execution. Hence, the cost of the MMI is lowered. Furthermore, the IGBT modules are compact in nature, hence the overall size of the MMI is lowered. Due to its compact feature, MMIs can be installed at the rear side of the PV panel. However, the MMI does not cover any more space for its installation. Another peculiar feature of the MMI is that it does not need any auxiliary circuit to produce the negative voltage levels. Once the suggested inverter is developed, the solar photovoltaic panel is linked to it, and the obtained AC power from MMI is then fed to the induction motor. A speed sensor measures the motor's speed, and this information is provided to the controller which uses pulse width modulation to generate appropriate switching pulses for the inverter switches. The performance of the proposed system is tested with PI and fuzzy controllers. Settling time and reduced harmonics were assured while comparing the FL-based controller to the PI controller. Reducing the steady-state inaccuracy of the induction motor speed control is the major benefit of the suggested control technique. Steady-state inaccuracy creates harmonics at the output voltage of modular multilevel inverter. Thereby creating ripples in the stator voltage and current. From the results, it is concluded that the fuzzy controller performs best than the PI controller in improving power quality.

Declarations

Conflict of interest All the authors declare that we have no conflict of interest.

Ethical approval This article does not contain any studies with human participants or animals performed by any of the authors.

References

1. Lan H, Bai Y, Wen S, Yu DC, Hong Y-Y, Dai J, Cheng P (2016) Modeling and stability analysis of hybrid PV/diesel/ESS in ship power system. Inventions 1(5):1–16. https://doi.org/10.3390/inventions1010005

2. Jayasinghe SG, Meegahapola L, Fernando N, Jin Z, Guerrero JM (2017) Review of ship microgrids: system architectures, storage technologies and power quality aspects. Inventions 2(4):1–19. https://doi.org/10.3390/inventions2010004

3. Kumar R, Singh B (2017) Single stage solar PV fed brushless DC motor driven water pump. IEEE J Emerg Select Topic Power Electron 5(3):1337–1385. https://doi.org/10.1109/JESTPE.2017.2699918

4. Shukla S, Singh B (2018) Single stage PV array fed speed sensorless vector control of induction motor drive for water pumping. IEEE Trans Ind Appl 54(4):1–10. https://ieeexplore.ieee.org/document/8304696

5. Singh B, Sharma U, Kumar S (2018) Standalone photovoltaic water pumping system using induction motor drive with reduced sensors. IEEE Trans Ind Appl 54(4):1–9. https://doi.org/10.1109/TIA.2018.2825285

6. Shunmugham Vanaja D, Stonier AA (2021) Grid integration of modular multilevel inverter with improved performance parameters. Int Trans Electr Energy Syst 31(1):e12667. https://doi.org/10.1002/2050-7038.12267

7. Shunmugham Vanaja D, Albert JR, Stonier AA (2021) An experimental investigation on solar PV fed modular STATCOM in WECS using Intelligent controller. Int Trans Electr Energy Syst 31(5):e12845. https://doi.org/10.1002/2050-7038.12845

8. Long W, Liu N, Wang K, Xu X, Zheng Z, Li Y A modular multilevel converter with integrated composite energy storage for ship MVDC electric propulsion system. In: 2020 IEEE 9th international power electronics and motion control conference (IPEMC2020-ECCE Asia), IEEE, pp 824–829. https://doi.org/10.1109/IPEMC-ECCEAsia48364.2020.9367843

9. Li C (2021) Comparison and analysis of improved NLM strategy for modular multilevel converter in ship medium voltage DC power system. Int Core J Eng 7(4):307–316. https://doi.org/10.6919/ICJE.202104_7(4).0042

10. Vechalapu K, Bhattacharya S (2015) Modular multilevel converter based medium voltage DC amplifier for ship board power system. In: 2015 IEEE 6th international symposium on power electronics for distributed generation systems (PEDG), IEEE, pp 1–8. https://doi.org/10.1109/PEDG.2015.7223098

11. Kakar S, Ayob SBM, Iqbal A, Nordin NM, Arif MSB, Gore S (2021) New asymmetrical modular multilevel inverter topology with reduced number of switches. IEEE Access 9:27627–27637. https://doi.org/10.1109/ACCESS.2021.3057554

12. Long W, Liu N, Wang K, Zheng Z, Li Y (2019) symmetrical hybrid multilevel inverters for ship electric propulsion drives. In: 2019 IEEE 4th international future energy electronics conference (IFEEC), IEEE, pp 1–6. https://doi.org/10.1109/IFEEC47410.2019.9015090

13. Xu X, Liu N, Wang K, Zheng Z, Li Y (2019) Modulation and control of an ANPC/H-bridge hybrid inverter for ship electric propulsion drives. In: 2019 22nd international conference on electrical machines and systems (ICEMS), IEEE, pp 1–5. https://doi.org/10.1109/ICEMS.2019.8922323

14. Giannoutsos SV, Manias SN (2014) A systematic power quality assessment and harmonic filter design methodology for variable frequency drive application in marine vessels. IEEE Trans Ind Appl 51(2):1909–1919. https://doi.org/10.1109/TIA.2014.2347453

15. Chunduri R, Benisha Gracelin D, ShunmughamVanaja D, Priyadarshini S, Khillo A, Ganthia BP (2021) Design and control of a solar photovoltaic fed asymmetric multilevel inverter using computational intelligence. Ann Roman Soc Cell Biol 25(6):10471–10484

16. Shunmugham Vanaja D, Stonier AA (2020) A novel PV fed asymmetric multilevel inverter with reduced THD for a grid-connected system. Int Trans Electr Energy Syst 30(4):e12267. https://doi.org/10.1002/2050-7038.12667

17. Thangaraj R, Chelliah TR, Pant M, Abraham A, Grosan C (2011) Optimal gain tuning of PI speed controller in induction motor drives using particle swarm optimization. Logic J IGPL 19(2):343–356. https://doi.org/10.1093/jigpal/jzq031

18. Albert JR, Vanaja DS (2020) Solar energy assessment in various regions of Indian sub-continent. Solar Cells. IntechOpen. https://doi.org/10.5772/intechopen.95118

19. El Geneidy R, Otto K, Ahtila P, Kujala P, Sillanpaa K, Mäki-Jouppila T (2018) Increasing energy efficiency in passenger ships by novel energy conservation measures. J Marin Eng Technol 17(2):85–98. https://doi.org/10.1080/20464177.2017.1317430

20. El Ouanjli N, Derouich A, El Ghzizal A, Chebabhi A, Taoussi M (2017) A comparative study between FOC and DTC control of the doubly fed induction motor (DFIM). In: IEEE international conference in electrical and information technologies, ICEIT, pp 1–6. https://doi.org/10.1109/EITech.2017.8255302

21. Abderazak S, Farid N (2016) Comparative study between Sliding mode controller and Fuzzy Sliding mode controller in a speed control for doubly fed induction motor. In: IEEE 4th international conference in control engineering and information technology, pp 1–6. https://doi.org/10.1109/CEIT.2016.7929044

22. Abdellatif M, Debbou M, Slama-Belkhodja I, Pietrzak-David M (2014) Simple low-speed sensorless dual DTC for double fed induction machine drive. IEEE Trans Ind Electron 61(8):3915–3922. https://doi.org/10.1109/TIE.2013.2288190